Available online at www.sciencedirect.com

ScienceDirect

Ceramics International 40 (2014) 629–635

CERAMICS INTERNATIONAL

www.elsevier.com/locate/ceramint

Effects of different synthesizing processes on the dielectric and piezoelectric properties of $0.65(K_{0.5}Bi_{0.5}TiO_3)$–$0.35BaTiO_3$ ceramics

Ping-Shou Cheng[a], Ying-Hsun Lin[a], Yuan-Tai Hsieh[b], Cheng-Fu Yang[c,*]

[a]Department of Electronic Engineering, National Kaohsiung University of Applied Sciences, Kaohsiung, Taiwan, ROC
[b]Department of Electronic Engineering, Southern Taiwan University, Tainan, Taiwan, ROC
[c]Department of Chemical and Materials Engineering, National University of Kaohsiung, Kaohsiung, Taiwan, ROC

Received 4 April 2013; received in revised form 12 June 2013; accepted 12 June 2013
Available online 19 June 2013

Abstract

In this study, $0.65(K_{0.5}Bi_{0.5})TiO_3$–$0.35BaTiO_3$ (KBT–BT3) ceramics were synthesized using two different methods: a conventional calcination process (CC-process) and a two-step calcination process that combined hydrothermal and CC processes (HT–CC-process). The effects of the differently synthesizing processes on the physical and dielectric properties of the KBT–BT3 ceramics were recorded and analyzed. Two secondary phases, BaBi4Ti4O15 and K4Ti3O8, were observed in the XRD patterns of the CC-process KBT–BT3 ceramics. The formations of $BaBi_4Ti_4O_{15}$ and $K_4Ti_3O_8$ compounds made the CC-process KBT–BT3 ceramics having poor dielectric properties. When the HT–CC-process was used and the KBT–BT3 ceramics were sintered at 1050–1100 °C, the secondary phases were not observed and only the $(K_{0.5}Bi_{0.5}, Ba)TiO_3$ phase was observed in the XRD patterns. As same sintering temperature was used, the dielectric constants of the HT–CC-process KBT–BT3 ceramics were higher than those of the CC-process KBT–BT3 ceramics. Electromechanical coupling factors, such as the planar coupling factor (k_p), thickness coupling factor (k_t), and longitudinal coupling factor (k_{33}), were also used to explain the effect of the different synthesizing processes on the properties of the KBT–BT3 ceramics.

Keywords: $K_{0.5}Bi_{0.5}TiO_3$ ceramics; Hydrothermal; Piezoelectric property; Dielectric property

1. Introduction

Perovskite-structured lead zirconate titanate (PZT)-based ceramics have been widely used in actuators, sensors, resonators, transducers, and transformers because of their excellent piezoelectric and electrical properties [1,2]. However, during the fabrication process of PZT-based ceramics the PbO has a problem of high volatility, and PbO will contaminate the environment and damage the human health. With the global rise in environmental consciousness, lead-free materials, such as Bi-based [3–5] and alkaline niobate compounds [6,7], have attracted much attention and are investigated to replace the PZT-based piezoelectric materials.

$K_{0.5}Bi_{0.5}TiO_3$ (KBT) ceramic is a typical Pb-free ferroelectric material. KBT has a perovskite structure and a relatively high Curie temperature (T_c=380–385 °C), and it can be developed for the applications of filters, resonators, and micro-electro-mechanical systems (MEMS) [8]. But it is difficult to fabricate KBT ceramics with high density using a traditional solid-state reaction method because Bi_2O_3 is highly volatile during the fabrication process. Vaporization of Bi_2O_3 leads to the formation of secondary or unknown phases [9], and the dielectric property of KBT-based ceramics will be degenerated [10].

Recently, hydrothermal synthesis was clearly identified as an important technology for synthesizing materials, predominantly in the fields of hydrometallurgy and single crystal growth [11]. However, only few reports have been published on KBT-based ceramics fabricated using hydrothermal synthesis. In this study,

*Correspondence to: No.700, Kaohsiung University Rd., 821, Nantzu District, Department of Chemical and Materials Engineering, National University of Kaohsiung, Kaohsiung, Taiwan, R.O.C.
E-mail address: cfyang@nuk.edu.tw (C.-F. Yang).

0272-8842/$ - see front matter
http://dx.doi.org/10.1016/j.ceramint.2013.06.046

0.65 $K_{0.5}Bi_{0.5}TiO_3$–0.35$BaTiO_3$ (KBT–BT3) was used as the main composition. At first, KBT–BT3 ceramics were synthesized by a traditional solid-state reaction method. In order to obtain the high-densified ceramics and inhibit the formation of secondary or unknown phases, a method combining the hydrothermal and solid-state reaction processes was developed. We would propose an explanation for why the calcination process had an important influence on the crystallization, morphology, and dielectric properties of the KBT–BT3 ceramics. The piezoelectric properties, such as the planar coupling factor (k_p), thickness coupling factor (k_t), and longitudinal coupling factor (k_{33}), were also used to explain how the different synthesis processeses would influence the properties of the KBT–BT3 ceramics.

2. Experimental

2.1. Conventional calcination process (CC-process)

Reagent-grade K_2CO_3, Bi_2O_3, $BaTiO_3$, and TiO_2 with purity higher than 99.5% were used as the raw materials to form the required composition, according to the formula of 0.65 ($Bi_{0.5}K_{0.5}TiO_3$)–0.35($BaTiO_3$). After being ball-milled in an agate mortar with deionized water for 2 h, the mixed powders were dried, ground, and calcined at 850 °C for 2 h.

2.2. Two-step process: combining the hydrothermal and CC processes (HT–CC-process)

For the HT–CC-process, the raw materials were also used to form the formula of 0.65($Bi_{0.5}K_{0.5}TiO_3$)–0.35($BaTiO_3$), and then the KBT–BT3 powder was put into a 100 mL Teflon-lined autoclave with a filling factor of approximately 80 vol%. The autoclave was heated in a furnace at 200 °C for 2 h. Following the hydrothermal process, the autoclave was cooled at room temperature, and then the powder was dried, ground, and calcined at 850 °C for 2 h.

2.3. Ceramic preparation and measurements

The CC-process and HT–CC-process KBT–BT3 powders were ground and uniaxially pressed into pellets of 1 mm thickness and 11.5 mm diameter using a steel die. The pellets were sintered at 1050–1125 °C for 2 h, then their crystallization structures were recorded using X-ray diffraction (XRD) patterns and grazing incidence angle X-ray diffraction (GIAXRD) patterns, and micrographs were observed using field-emission scanning electron microscope (FESEM). To measure the electrical properties, silver paste was painted on both sides of the KBT–BT3 ceramics to form electrodes, the painted ceramics were then fired at 700 °C for 15 min. The dielectric properties were measured using an HP 4294 impedance analyzer. After that, the KBT–BT3 ceramics were placed into a temperature-programmable testing chamber. The measured temperature range was changed from 30 °C to 500 °C, and the temperature-dependent dielectric characteristics (ε_r–T) were obtained. The piezoelectric properties were also measured after pooling the KBT–BT3 ceramics under a 3 kV/mm dc field at 150 °C in silicon oil for 30 min. The KBT–BT3 ceramics were measured at room temperature and the measured frequency was changed from 10 KHz to 1 MHz to find the resonance frequency (f_r) and the anti-resonance frequency (f_a). The values of planar coupling factor (k_p), thickness (k_t) coupling factor, and longitudinal coupling factor (k_{33}) were calculated using the resonance and anti-resonance method.

3. Results and discussion

Fig. 1 shows the XRD patterns of the CC-process and HT–CC-process KBT–BT3 ceramics as a function of sintering temperature, it clearly revealed that the differently synthesizing processes created different results. As the sintering temperature of the CC-process and HT–CC-process KBT–BT3 ceramics was increased from 1050 °C to 1125 °C, no shift in the 2θ values of the mainly crystalline (101) peak was observed. This result suggests that $BaTiO_3$ and $K_{0.5}Bi_{0.5}TiO_3$ were formed a homogeneous solid solution in 0.65($K_{0.5}Bi_{0.5}$)TiO_3–0.35$BaTiO_3$ composition. In addition, as 1050°C was used as sintering temperature and the 2θ value between 44° and 48° was compared, the KBT–BT3 ceramics obtained from both methods presented a cubic structure; As the sintering temperature was increased from 1075 °C to 1100 °C, the crystalline structure showed that the KBT–BT3 ceramics were transformed into the tetragonal phase. However, as the sintering temperature was increased, the secondary $BaBi_4Ti_4O_{15}$ phase was observed in the 1075 °C-, 1100 °C-, and 1125 °C-sintered CC-process KBT–BT3 ceramics, and its diffraction intensity increased with raising sintering temperature. The secondary $K_4Ti_3O_8$ phase was also observed in the 1100 °C- and 1125 °C-sintered CC-process KBT–BT3 ceramics. The ideal reaction equation for the KBT–BT3 ceramics is:

$$0.175K_2CO_3 + 0.175Bi_2O_3 + 0.65BaCO_3 + TiO_2 \rightarrow (K_{0.5}Bi_{0.5},\ Ba)TiO_3 + CO_2\uparrow \quad (1)$$

The $BaBi_4Ti_4O_{15}$ phase may be caused by residual Bi_2O_3, TiO_2, and $BaCO_3$, as in the following equation:

$$Bi_2O_3 + BaCO_3 + TiO_2 \rightarrow BaBi_4Ti_4O_{15} + CO_2\uparrow \quad (2)$$

As reported by Zhu et al. [8], the appearance of the secondary $K_4Ti_3O_8$ phase is due to the evaporation of bismuth. For that, the following reaction occurs and the $K_4Ti_3O_8$ phase will be revealed in the 1100 °C- and 1125 °C-sintered CC-process KBT–BT3 ceramics:

$$K_{0.5}Bi_{0.5}TiO_3 \rightarrow K_4Ti_3O_8 + Bi_2O_3\uparrow \quad (3)$$

Conversely, the KBT–BT3 ceramics that treated using the HT–CC-process had fewer secondary phases than those that treated using the CC-process. Sintered at 1050–1100 °C, only the ($K_{0.5}Bi_{0.5}$, Ba)TiO_3 phase was observed in the XRD patterns of the HT–CC-process ceramics. As the sintering temperature was raised to 1125 °C, the $BaBi_4Ti_4O_{15}$ phase was also observable in the XRD patterns of the HT–CC-process ceramics. These results demonstrate that the HT–CC-process can inhibit the secondary phases formed during the sintering process. In the past literatures, the differently secondary phases were formed in the KBT ceramics as different synthesized

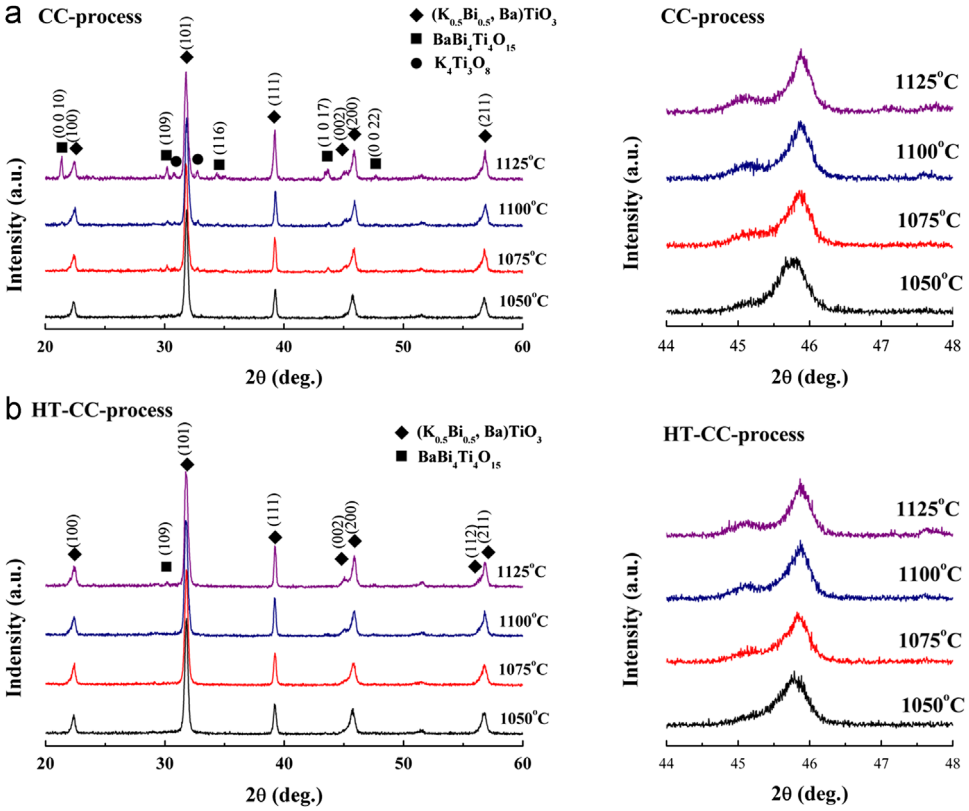

Fig. 1. XRD patterns of the (a) CC-process and (b) HT–CC-process KBT–BT3 ceramics.

processes were used. For example, the $K_4Ti_3O_8$ phase was formed in the sol–gel-hydrothermal synthesis method [12], the $K_2Ti_6O_{13}$ phase was formed in the hot-pressing method [13], and $K_2Ti_6O_{13}$ and $K_2Ti_4O_9$ were formed in the solid-state method [14]. These results again suggest that for KBT–BT3 ceramics, the HT–CC-process is a better synthesis method than the CC-process and the processes in the past literatures.

The main diffraction peaks of $BaBi_4Ti_4O_{15}$ ceramics existing in the range of 20–60° are (0,0,10), (1,0,9), and (1,1,6) for 2θ values at around 21.4°, 30.2°, and 34.4° respectively, and the mainly diffraction peaks for $K_4Ti_3O_8$ ceramics are (0,0,10) and (1,1,6) for 2θ values at around 30.8° and 32.7°, respectively [15]. In the past, the grazing incidence angle X-ray diffraction (GIAXRD) patterns were the proper and powerful method used to identify the crystalline structures of the nanoparticles and thin films [16]. For that, the GIAXRD was used and analyzed for 2θ values in the ranges of 20–24° and 28–35° to confirm the existence of secondary phases in the CC-process and HT–CC-process KBT–BT3 ceramic. From the results shown in Fig. 2, the $BaBi_4Ti_4O_{15}$ and $K_4Ti_3O_8$ phases were really observed in the 1075–1125 °C-sintered CC-process KBT–BT3 ceramics, and their diffraction intensities increased with increasing sintering temperature. For the HT–CC-process KBT–BT3 samples, only the secondary $BaBi_4Ti_4O_{15}$ phase was observed in the 1125 °C-sintered ceramics.

Fig. 3 shows SEM micrographs of the CC-process and HT–CC-process KBT–BT3 ceramics. The micrographs of the 1075 °C-sintered CC-process and HT–CC-process KBT–BT3 ceramics (Fig. 3(a) and (d)) show a porous structure and grain growth was not apparently observed. This result indicates that 1075 °C is not high enough for KBT–BT3 ceramics to form a dense structure and improve grain growth. As the sintering temperature was increased to 1100 °C and 1125 °C, the grain growths were apparently improved and no pores were observed (Fig. 3(b), (c), (e), and (f)). The average grain sizes of the 1075–1125 °C sintered CC-process and HT–CC-process KBT–BT3 ceramics were in the ranges of 0.4–1.2 μm and 0.3–0.94 μm, respectively. Although the average grain sizes of the HT–CC-process KBT–BT3 ceramics were smaller than those of the CC-process ones, both methods yielded very similar results in the surface morphologies. This indicates that the HT—CC-process has no apparent effect to improve the grain growth mechanism of the KBT–BT3 ceramics.

Fig. 4 compares the temperature-dependent relative dielectric constant (ε_r-T) curves of the CC-process and HT–CC-process KBT–BT3 ceramics as a function of sintering temperature. As the measured temperature increased, the ε_r values gradually increased to a maximum value at Curie temperature and then decreased, a transition from the ferroelectric phase to the paraelectric phase is the reason. The Curie temperatures (T_c, the temperature revealing the maximum dielectric constant) of the CC-process and HT–CC-process KBT–BT3 ceramics were also observed in Fig. 4. The T_c values of the CC-process KBT–BT3 ceramics were 340 °C, 310 °C, 300 °C, and 320 °C as the sintering temperatures were 1050 °C, 1075 °C, 1100 °C, and 1125 °C, respectively. From the XRD

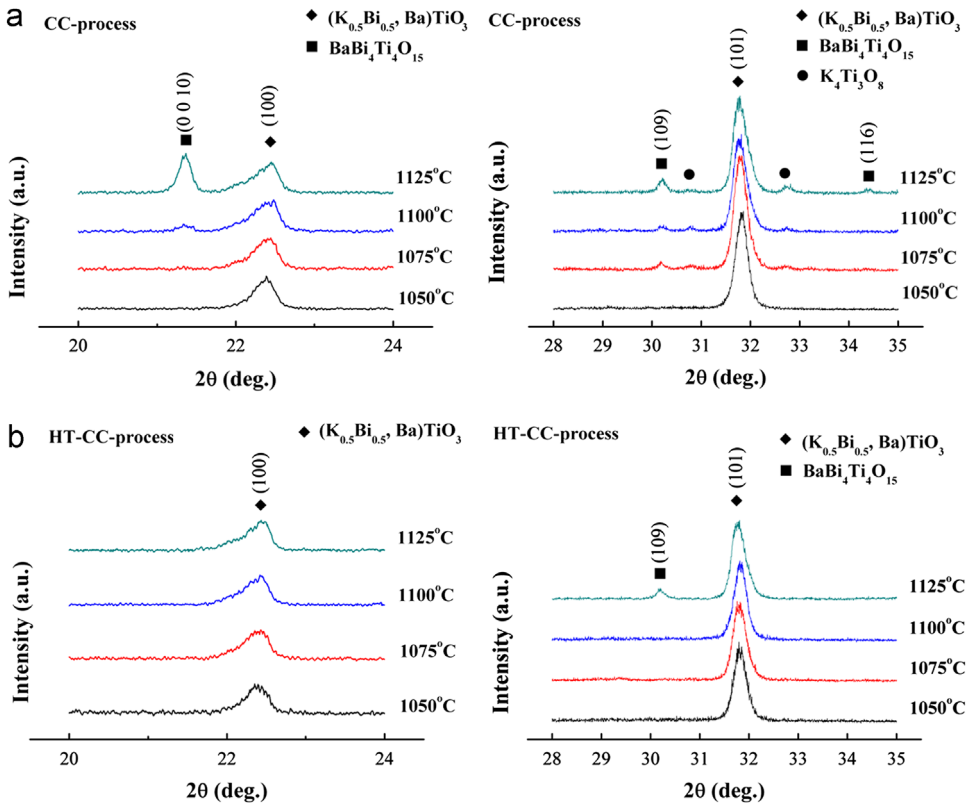

Fig. 2. GIAXRD patterns of the CC-process and HT–CC-process KBT–BT3 ceramics.

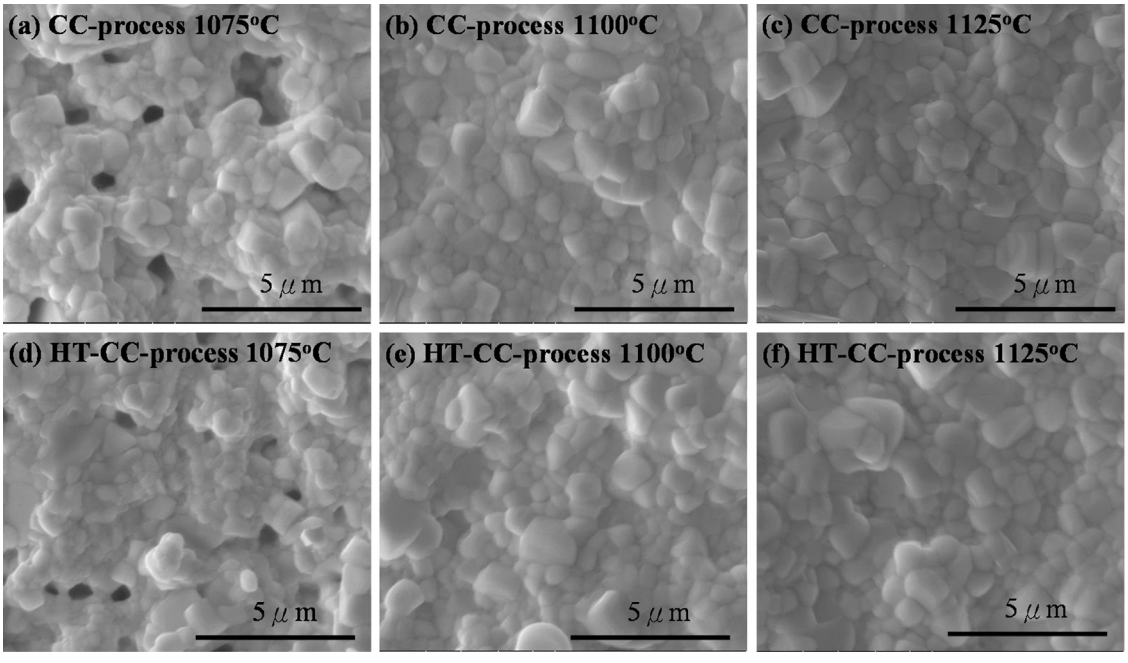

Fig. 3. Surface morphologies of the KBT–BT3 ceramics: (a), (b), and (c) CC-process; (c), (d), and (e) HT–CC-process.

analysis in Fig. 1(a), the reason for the large T_c variation in the CC-process KBT–BT3 ceramics is attributed to coexistence of the secondary phases of $BaBi_4Ti_4O_5$, which has a T_c value of 425–430 °C [17,18]. In comparison, the T_c values of the HT–CC-process KBT–BT3 ceramics virtually remained at 280–290 °C as the sintering temperature increased from 1050 °C to 1100 °C. As sintered at 1125 °C, the T_c value of the HT–CC-process KBT–BT3 ceramics was increased to 340 °C. Based on the XRD analysis shown in Fig. 1 and the GIAXRD analysis in Fig. 2, the formation of $BaBi_4Ti_4O_5$ phase in the XRD patterns of the 1125 °C-sintered HT–CC-process KBT–BT3 ceramics is the reason to cause this result.

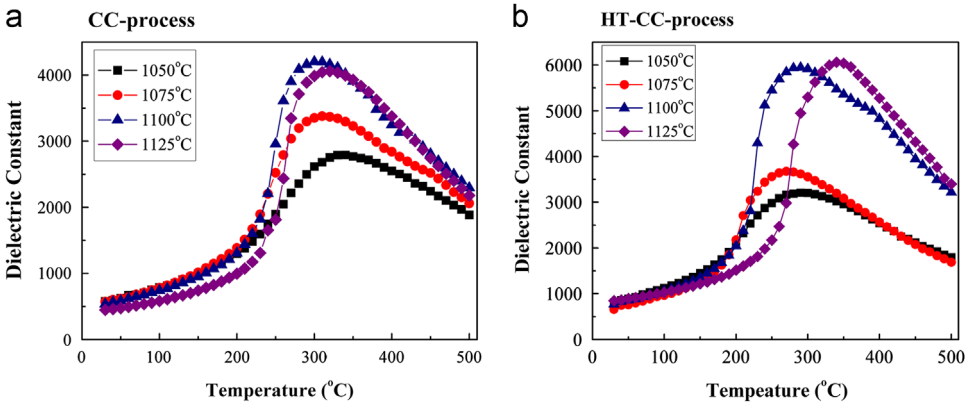

Fig. 4. Comparison of the ε_r–T curves of the CC-process and HT–CC-process KBT–BT3 ceramics.

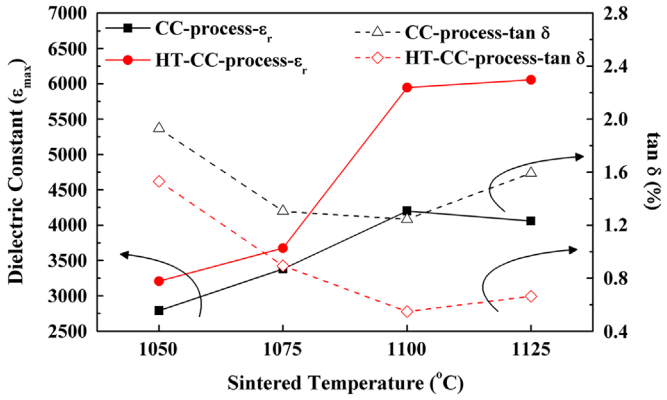

Fig. 5. Comparison of the ε_{max} and tan δ values of the CC-process and HT–CC-process KBT–BT3 ceramics.

The maximum dielectric constants (ε_{max}, revealed at Curie temperature) and loss tangents (tan δ, revealed at ε_{max} peak) of the CC-process and HT–CC-process KBT–BT3 ceramics are measured at 1 MHz and the results are shown in Fig. 5 as a function of sintering temperature. When 1050 °C was used as sintering temperature, the ε_{max} values of the CC-process and HT–CC-process KBT–BT3 ceramics were 2790 and 3208; As the sintering temperature was raised to 1100 °C, the ε_{max} values were 4202 and 5946, respectively. Fig. 5 also shows that as the same sintering temperature was used, the ε_{max} values of the CC-process KBT–BT3 ceramics were all lower than those of the HT–CC-process ones. These results demonstrate that the HT–CC-process method effectively improve the dielectric constants of the KBT–BT3 ceramics. As sintering temperature was raised, the tan δ values initially decreased, and 1100 °C-sintered CC-process and HT–CC-process KBT–BT3 ceramics had the lowest tan δ values. Those stated results conclude that 1100 °C is the optimum sintering temperature in this literature, because the CC-process and the HT–CC-process KBT–BT3 ceramics sintered at this temperature have higher dielectric constants and the lowest tan δ values.

Many factors can influence dielectric characteristics of ceramics, including (1) grain growth, (2) doping concentration, (3) pore ratio, and (4) materials having a phase with low dielectric constant. In this study, the dominant factors are (1), (3), and (4). The SEM micrographs in Fig. 3 indicate that as the sintering temperature was raised, the elimination of pores and improvement in grain growth caused the increase in ε_{max} values, while the improvement in tan δ values was also due to the same reasons. However, Fig. 5 shows that as the same sintering temperature was used, the tan δ values of the CC-process KBT–BT3 ceramics were all larger than those of the HT–CC-process ceramics. Generally, secondary phases existing in a ceramic will degenerate a ceramic's dielectric constant because of their lower dielectric constants. For example, $BaBi_4Ti_4O_{15}$ ceramic measured at 1 MHz has a lower dielectric constant of 2500–3000 [16]. The reasons are based on the XRD and GIAXRD patterns compared in Figs. 1 and 2 that the secondary $BaBi_4Ti_4O_{15}$ phase is formed in the CC-process KBT–BT3 ceramics. As Figs. 1 and 2 show, even when the sintering temperature is raised to 1125 °C, less of the secondary phase exists in the HT–CC-process KBT–BT3 ceramics. These results also prove that the HT–CC-process not only can inhibit the formation of secondary phases but also can synthesize KBT–BT3 ceramics with superior dielectric properties.

Fig. 6 shows the frequency dependencies on the impedance $|Z|(\Omega)$ of the CC-process and HT–CC-process KBT–BT3 ceramics. The variation ranges in the impedance of the CC-process and HT–CC-process KBT–BT3 ceramics gradually increased with the raising of sintering temperature. Fig. 3 really shows that as sintering temperature increased from 1050 °C to 1100 °C, the pores apparently decreased and no pores were observed in the 1100 °C-sintered KBT–BT3 ceramics. Fig. 3 also shows that the increase of sintering temperature had no apparent effect on grain growth because the grain sizes slightly increased as sintering temperature increased from 1075 °C to 1100 °C. However, the decrease in pores and the increase in grain size are two reasons to cause the increase of structural density. On the basis of these results, the optimum sintering temperature for both methods should be higher than 1075 °C.

The piezoelectric planar (k_p) and thickness (k_t) coupling factors can be calculated by the following equation [19]:

$$\frac{1}{k^2} = a \times \frac{f_r}{f_a - f_r} + b \tag{4}$$

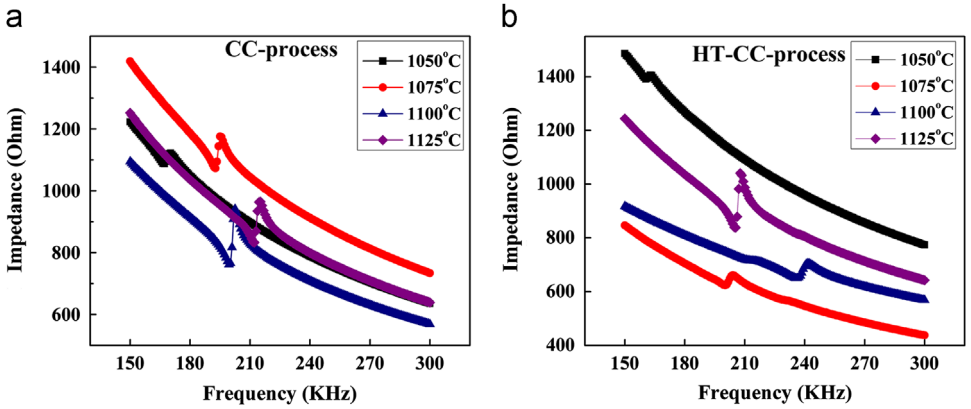

Fig. 6. Frequency dependence on the impedances of the 1050–1125 °C sintered CC-process and HT–CC-process KBT–BT3 ceramics.

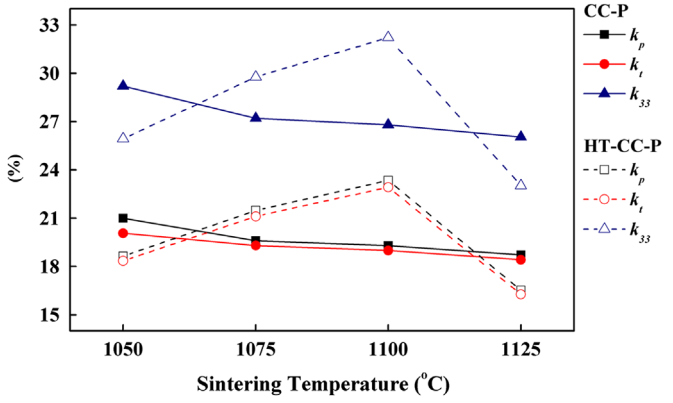

Fig. 7. k_p, k_t, and k_{33} of the CC-process and HT–CC-process KBT–BT3 ceramics.

where f_r is the resonance frequency and f_a is the anti-resonance frequency. The planar (k_p) factor can be estimated by using $a=0.395$ and $b=0.574$ for, and the thickness (k_t) factor can be estimated by using $a=0.405$ and $b=0.810$. The longitudinal coupling factor, k_{33}, can be estimated from the piezoelectric planar and thickness coupling factors [20]:

$$k_{33}^2 = k_p^2 + k_t^2 - k_p^2 k_t^2 \quad (5)$$

Variations in the k_p, k_t, and k_{33} values for the CC-process and HT–CC-process KBT–BT3 ceramics are shown in Fig. 7 as a function of sintering temperature. The k_p, k_t, and k_{33} values of the CC-process KBT–BT3 ceramics decreased as the sintering temperature raised. In contrast, the k_p, k_t, and k_{33} values of the HT–CC-process KBT–BT3 ceramics first increased as sintering temperature increased, and they reached the maximum values of 23.34%, 22.92%, and 32.22% at 1100 °C. This significant enhancement in the piezoelectric properties of the HT–CC-process KBT–BT3 ceramics is due to two factors: (1) the optimum sintering temperature for grain growth at 1100 °C increased the ceramics' density, lowered the tan δ values, and enhanced the poling results; (2) comparing the results from the XRD patterns in Fig.1 and 2 only the $(K_{0.5}Bi_{0.5}, Ba)TiO_3$ phase was formed. Also, the decrease in pores and the increase in grain size are the reasons to enhance the piezoelectric properties. If we consider the XRD pattern and GIAXRD patterns of the 1125 °C-sintered HT–CC-process KBT–BT3 ceramics, the secondary $BaBi_4Ti_4O_{15}$ phase is considered as the theorem to cause the decreases in k_p, k_t, and k_{33} values of the 1125 °C-sintered CC-process KBT–BT3 ceramics.

4. Conclusions

In this study, $0.65K_{0.5}Bi_{0.5}TiO_3$–$0.35BaTiO_3$ (KBT–BT3) ceramics synthesized using different calcination methods were thoroughly investigated. As the CC- and HT–CC-calcination processes were used, 1075 °C was not high enough for KBT–BT3 ceramics to form a dense structure and improve grain growth; As 1100 °C and 1125 °C were used as sintering temperatures, the grain growths were apparently improved and no pores were observed. The poor dielectric and piezoelectric properties of the CC-process KBT–BT3 ceramics were due to the appearance of secondary phases, such as $BaBi_4Ti_4O_{15}$ and $K_4Ti_3O_8$. The average grain sizes of the HT–CC-process KBT–BT3 ceramics were smaller than those of the CC-process ceramics, both methods yielded very similar results in the surface morphologies. As the same sintering temperature was used, the HT–CC-process KBT–BT3 ceramics had more superior dielectric and piezoelectric properties because only the $(K_{0.5}Bi_{0.5}, Ba)TiO_3$ phase was formed. Analysis of the piezoelectric properties showed that the k_p, k_t, and k_{33} values of the CC-process KBT–BT3 ceramics were lower than those of the HT–CC-process ceramics due to the coexistence of the secondary $BaBi_4Ti_4O_{15}$ and $K_4Ti_3O_8$ phases. The optimal k_p (23.34%), k_t (22.92%), and k_{33} (32.22%) values were obtained in the 1100 °C-sintered HT–CC-process KBT–BT3 ceramics. On the basis of the above results, we consider the HT–CC process a potential method for synthesizing the KBT–BT3 ceramics.

References

[1] Z. Yang, X. Chao, R. Zhang, Y. Chang, Y. Chen, Fabrication and electrical characteristics of piezoelectric PMN–PZN–PZT ceramic transformers, Materials Science and Engineering 138 (2007) 277–283.

[2] C.W. Ahn, H.C. Song, P. Shashank, P.S. Ho, K. Uchino, H.G. Lee, H.J. Lee, Effect of ZnO and CuO on the sintering temperature and piezoelectric properties of a hard piezoelectric ceramic, Journal of the American Ceramic Society 89 (2006) 921–925.
[3] T. Takenaka, T. Gotoh, S. Mutoh, T. Sasaki, A new series of bismuth layer-structured ferroelectrics, Japanese Journal of Applied Physics 34 (1995) 5384–5388.
[4] M. Hirose, T. Suzuki, H. Oka, K. Itakura, Y. Miyauchi, T. Tsukada, Piezoelectric properties of $SrBi_4Ti_4O_{15}$-based ceramics, Japanese Journal of Applied Physics 38 (1999) 5561–5563.
[5] G. Fan, W. Lu, X. Wang, F. Liang, J. Xiao, Phase transition behaviour and electromechanical properties of $(Na_{1/2}Bi_{1/2})TiO_3$–$KNbO_3$ lead-free piezoelectric ceramics, Journal of Physics D: Applied Physics 41 (2008) 035403–035409.
[6] G.H. Haertling, Ferroelectric ceramics: history and technology, Journal of the American Ceramic Society 82 (1999) 797–818.
[7] H.E. Mgbemere, R.P. Herber, G.A. Schneider, Effect of MnO_2 on the dielectric and piezoelectric properties of alkaline niobate based lead free piezoelectric ceramics, Journal of the European Ceramic Society 29 (2009) 1729–1733.
[8] M. Zhu, L. Hou, Y. Hou, J. Liu, H. Wang, H. Yan, Lead-free $(K_{0.5}Bi_{0.5})TiO_3$ powders and ceramics prepared by a sol–gel method, Materials Chemistry and Physics 99 (2006) 329–332.
[9] C.F. Buhrer, Some properties of bismuth perovskites, Journal of Chemical Physics 36 (1962) 798–803.
[10] T. Zaremba, Application of thermal analysis to study of the synthesis of $K_{0.5}Bi_{0.5}TiO_3$ ferroelectric, Journal of Thermal Analysis and Calorimetry 74 (2003) 653–658.
[11] K. Byrappa, M. Yoshimura, Handbook of Hydrothermal Technology, Noyes Publications/William Andrew Publishing LLC, U.S.A., 2001.
[12] L. Hou, Y.D. Hou, X.M. Song, M.K. Zhu, H. Wang, H. Yan, Sol–gel-hydrothermal synthesis and sintering of $K_{0.5}Bi_{0.5}TiO_3$ nanowires, Materials Research Bulletin 41 (2006) 1330–1336.
[13] Y. Hiruma, R. Aoyagi, H. Nagata, T. Takenaka, Ferroelectric and piezoelectric properties of $(Bi_{1/2}K_{1/2})TiO_3$ ceramic, Japanese Journal of Applied Physics 44 (2005) 5040–5044.
[14] J. König, M. Spreitzer, B. Jaňcar, D. Suvorov, Z. Samarďzija, A. Popovǐc, The thermal decomposition of $K_{0.5}Bi_{0.5}TiO_3$ ceramics, Journal of the European Ceramic Society 29 (2009) 1695–1701.
[15] K.I. Chatchai, G. Rujijanagu, F.Y. Zhu, Steven J. Milne, Relaxor behaviour of $K_{0.5}Bi_{0.5}Nb_{O3}$–$BiScO_3$ ceramics, Applied Physics Letters 100 (2012) 202904.
[16] C.C. Wu, C.F. Yang, Investigation of the properties of nanostructured Li-doped NiO films using the modified spray pyrolysis method, Nanoscale Research Letters 8 (2013) 33.
[17] I. Pribošič, D. Makovec, M. Drofenik, Electric properties of donor- and acceptor-doped $BaBi_4Ti_4O_{15}$, Journal of the European Ceramic Society 21 (2000) 1327–1331.
[18] A. Chakrabarti, J. Bera, T.P. Sinha, Dielectric properties of $BaBi_4Ti_4O_{15}$ ceramic sproduced by cost-effective chemical method, Physica B 404 (2009) 1498–1502.
[19] M. Matsubara, T. Yamaguchi, K. Kikuta, S.I. Hirano, Effect of Li Substitution on the Piezoelectric Properties of Potassium Sodium Niobate Ceramics, Japanese Journal of Applied Physics 44 (2005) 6136–6142.
[20] Z. Yang, X. Chao, C. Kang, R. Zhang, Low temperature sintering and properties of piezoelectric PZT–PFW–PMN ceramics with $YMnO_3$ addition, Materials Research Bulletin 43 (2008) 38–44.